Anion-Directed Formation and Degradation of an Interlocked Metallohelicate

Ryo Sekiya,*,[†,§] Morihiko Fukuda,[‡] and Reiko Kuroda*,[†,‡,⊥]

[†]Department of Life Sciences, Graduate School of Arts and Sciences, The University of Tokyo, 3-8-1 Komaba, Meguro-ku, Tokyo 153-8902, Japan

[‡]Department of Biophysics and Biochemistry, Graduate School of Science, The University of Tokyo, 7-3-1 Hongo, Bunkyo-ku, Tokyo 113-0033, Japan

S *Supporting Information*

ABSTRACT: Although there are many examples of catenanes, those of more complex mechanically interlocked molecular architectures are rare. Additionally, little attention has been paid to the degradation of such interlocked systems into their starting complexes, although formation and degradation are complementary phenomena and are equally important. Interlocked metallohelicate, $[(Pd_2L_4)_2]^{8+}$ (2^{8+}), is a quadruply interlocked molecular architecture consisting of two mechanically interlocked monomers, $[Pd_2L_4]^{4+}$ (1^{4+}). 2^{8+} has three internal cavities, each of which encapsulates one NO_3^- ion (1:3 host−guest complex, $2{\supset}(NO_3|NO_3|NO_3)^{5+}$) and is characterized by unusual thermodynamic stability. However, both the driving force for the dimerization and the origin of the thermodynamic stability remain unclear. To clarify these issues, BF_4^-, PF_6^-, and OTf^- have been used to demonstrate that the dimerization is driven by the anion template effect. Interestingly, the stability of 2^{8+} strongly depends on the encapsulated anions ($2{\supset}(NO_3|NO_3|NO_3)^{5+} \gg 2{\supset}(BF_4|BF_4|BF_4)^{5+}$). The origins of this differing thermodynamic stability have been shown through detailed investigations to be due to the differences in the stabilization of the interlocked structure by the host−guest interaction and the size of the anion. We have found that 2-naphthalenesulfonate (ONs^-) induces the monomerization of $2{\supset}(NO_3|NO_3|NO_3)^{5+}$ via intermediate $2{\supset}(ONs|NO_3|ONs)^{5+}$, which is formed by anion exchange. On the basis of this finding, and using *p*-toluenesulfonate (OTs^-), the physical separation of $2{\supset}(NO_3|NO_3|NO_3)^{5+}$ and 1^{4+} as OTs^- salt was accomplished.
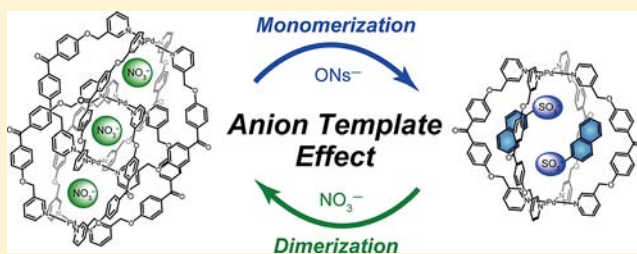
INTRODUCTION

Mechanically interlocked molecular architectures such as catenanes have received considerable attention because of their topologically interesting structures and their potential application to molecular machines.[1,2] Catenation requires the assembly of two or more macrocycles. Clearly, this process is entropically disfavored, and thus, for the rational synthesis of such interlocked systems, the understanding and control of structure-directing supramolecular interactions, such as hydrogen bonding, $\pi{\cdots}\pi$ interaction, and electrostatic interaction between the macrocycles or between the macrocycles and an auxiliary species (template), is of prime importance.

Catenanes have been synthesized by a number of methods.[1−6] Undoubtedly, the most prevalent method is the use of metal cations as templates, because their well-defined coordination geometries and metal−ligand coordination bonding are suitable for the association of components in a controllable manner.[1−3] An analogous approach using anionic species as templates also exists.[4,5] For example, Beer's group reported the rational synthesis of a purely organic interlocked system using a combination of the anion template effect and a click reaction.[5a] Catenanes can also be formed without the use of auxiliary template species. For example, Fujita's group reported that the fragment *cis*-$[M(en)_2]^{2+}$ (M = Pd^{2+}, Pt^{2+}; en =

ethylenediamine), along with bis-monodentate bridging ligands form M_2L_2-macrocycles, which self-assemble to give [2]-catenanes in almost quantitative yield with the aid of the hydrophobic effect and favorable interactions between the two macrocycles.[6]

Although there are many examples of catenanes, those of more complex interlocked molecular architectures, such as triply and quadruply interlocked molecular architectures, are rare.[5a,7,8] To the best of our knowledge, there are only three examples of quadruply interlocked species. One is a purely organic species that consists of two mechanically interlocked calix[4]arenes and was reported by Böhmer's group.[7f] The others were reported by us in 2008 (Figure 1)[8a] and very recently by Clever's group.[7i] In addition, little research has been carried out on the degradation of such interlocked complexes back to their starting complexes,[5o,p] though formation and degradation are complementary phenomena and are equally important, particularly in the fields of molecular machines and switches and supramolecular polymers.

The quadruply interlocked molecular architecture, an interlocked metallohelicate $[(Pd_2L_4)_2]^{8+}$ (2^{8+}), is formed by
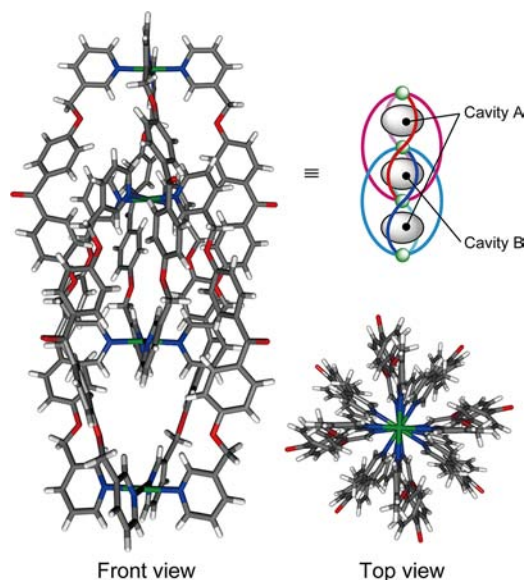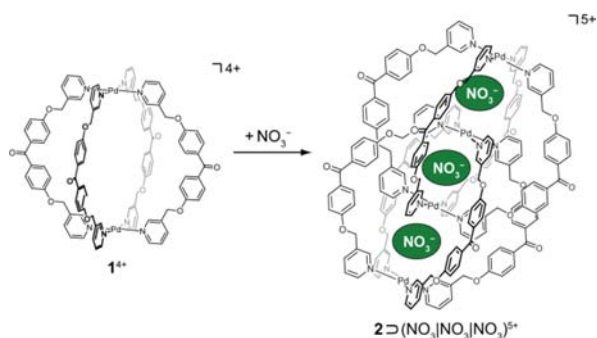
Figure 1. Front and top views of the X-ray crystal structure of 2^{8+} and a schematic representation of 2^{8+}.[8a] The counterion is NO_3^-. Color scheme: gray (carbon), white (hydrogen), blue (nitrogen), red (oxygen), green (palladium).

the spontaneous dimerization of monomers, $[Pd_2L_4]^{4+}$ (1^{4+}), in the presence of NO_3^- as a counterion (Scheme 1).[8a] X-ray

Scheme 1. Spontaneous Dimerization of 1^{4+} into $2\supset(NO_3|NO_3|NO_3)^{5+}$ in the Presence of NO_3^-

diffraction analysis revealed that 2^{8+} has three internal cavities (cavity A × 2 + cavity B × 1) with nearly equal volumes (ca. 62 Å^3, Figure 1)[9] and one NO_3^- ion encapsulated per cavity (Figure S1a in the Supporting Information). That is, 2^{8+} and the three NO_3^- ions form the 1:3 host–guest complex $2\supset(NO_3|NO_3|NO_3)^{5+}$ ("$\supset$" denotes encapsulation, and $(NO_3|NO_3|NO_3)$ denotes that the NO_3^- ions are encapsulated in (cavity A | cavity B | cavity A)). Electrospray ionization-mass spectrometry (ESI-MS) suggests that the three anions are tightly trapped in 2^{8+} (Figure S1b in the Supporting Information). $2\supset(NO_3|NO_3|NO_3)^{5+}$ is also characterized by its unusual thermodynamic stability.[8a] Under given reaction conditions (<80 °C), $2\supset(NO_3|NO_3|NO_3)^{5+}$ barely monomerizes; however, it decomposes slowly to monomers when it is subjected to heating at high temperature (>90 °C) for several hours. Interestingly, the resulting monomers are almost completely converted back to $2\supset(NO_3|NO_3|NO_3)^{5+}$ in DMSO-d_6 at room temperature.[8a] This re-formation is remarkable, because dimerization is an entropically unfavorable process, and in some cases, such as Fujita's [2]catenanes, the

aid of the hydrophobic effect is indispensable for the complete conversion of the macrocycles into the interlocked species.[6] This behavior implies that a strong structure-directing supramolecular interaction is operating and stabilizes the interlocked structure. To date, however, neither the driving force for the dimerization nor the origin of the thermodynamic stability has been clarified.

On the basis of the above backgrounds, we aimed to elucidate the driving force for the dimerization and the origin of the thermodynamic stability of $2\supset(NO_3|NO_3|NO_3)^{5+}$, particularly in relation to the encapsulated anions. In addition, we developed a method for the monomerization of $2\supset(NO_3|NO_3|NO_3)^{5+}$ by anions carrying a sulfonate group. Herein, we report the anion-directed formation and degradation of the interlocked metallohelicate.

■ RESULTS AND DISCUSSION

Preparation and X-ray Crystal Structure. To investigate the role of the anion in the dimerization, three anions Y^- ($Y^- = BF_4^-$, PF_6^-, and OTf^-) were employed. The synthesis of bis-monodentate bridging ligand L was reported previously.[8a] $1(Y)_4$ were synthesized by straightforward methods. The reaction of PdY_2 with 2 equiv of L in DMF at 60 °C for 1 h followed by the addition of Et_2O afforded $1(Y)_4$ as a white precipitate. $1(Y)_4$ are soluble only in DMSO and DMF.

^1H NMR and ESI-MS measurements confirmed the formation of 1^{4+}. The α-pyridyl protons H_a and H_b experience large downfield shifts due to the loss of electron density upon complexation with the Pd^{2+} centers (Figure 2a–c). (The signals
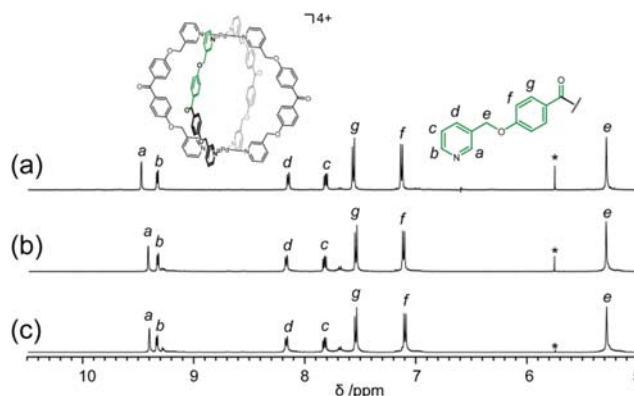

Figure 2. ^1H NMR spectra (500 MHz, DMSO-d_6, rt) of 1^{4+} in the presence of 4 equiv of (a) BF_4^-, (b) PF_6^-, and (c) OTf^-. The symmetrically independent part of 1^{4+} is colored with green. Asterisks denote CH_2Cl_2.

of H_a and H_b of free L appear at $\delta = 8.70$ and 8.54 ppm, respectively.[8a]) The highly symmetrical signal pattern (average D_{4h} symmetry on the NMR time scale) indicates rapid P-form $\leftrightarrow$ M-form inversion.[8b] The ESI-MS exhibits a series of ion peaks corresponding to $[1 + (Y)_n]^{4-n}$ ($n = 0–3$). Compared to the signal of H_a in the presence of PF_6^- or OTf^- ($\delta = 9.40$ ppm), that in the presence of BF_4^- appears at a more downfield region ($\delta = 9.51$ ppm), indicating host–guest complexation between 1^{4+} and BF_4^-.

$1(OTf)_4$ afforded single crystals for X-ray diffractometry. The colorless crystals of $1(OTf)_4$ grew slowly from a DMF solution of $1(OTf)_4$ at room temperature, following the diffusion of 1,4-dioxane vapor into the solution. Figure 3a shows the X-ray structure of 1^{4+} (triclinic, $P\bar{1}$).[10] The crystallographic
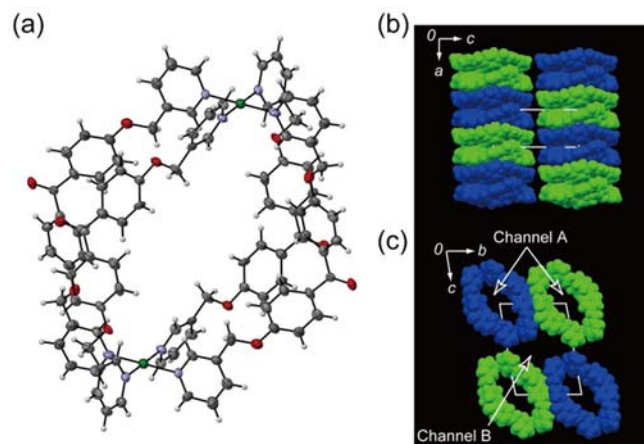
Figure 3. (a) ORTEP drawing (30% probability ellipsoids) of the X-ray crystal structure of 1^{4+}. The counterion is OTf$^-$. Color scheme: gray (carbon), white (hydrogen), blue (nitrogen), red (oxygen), green (palladium). (b and c) Space-filling illustrations of the crystal structure of 1^{4+} viewed along the [010] axis and the [100] axis, respectively. OTf$^-$ ions are not shown. In panels b and c, 1^{4+} is colored in blue or green.

Scheme 2. (a) Thermal Reactions of $1(PF_6)_4$ and $1(OTf)_4$,[a] (b) of $1(BF_4)_4$,[b] and (c) of $1(BF_4)_4$ with 4 equiv of NO_3^-, PF_6^-, and OTf$^-$ as the $(n\text{-}Bu)_4N^+$ Salts[c]

[a]No dimerization occurred. [b]The reaction afforded $2{\supset}(BF_4|BF_4|BF_4)^{5+}$ in 9.7% yield at the equilibrium state. [c]The reaction afforded $2{\supset}(NO_3|NO_3|NO_3)^{5+}$.

parameters are compiled in the Supporting Information. The symmetry of 1^{4+} is significantly lower than that of the complex in the solution. Most likely, this difference results from the flexible framework of 1^{4+} and packing effects; the stacking of 1^{4+} along the [100] axis "squashes" it (Figure 3b). C−H···π and π···π interactions are present between the neighboring bridging ligands. The Pd^{2+}/Pd^{2+} separation is 16.14 Å. There are two types of channels penetrating through the crystal (channel A and channel B, see Figure 3c). One of the two OTf$^-$ ions was located in channel B, without any interaction with the Pd^{2+} centers. The other OTf$^-$ ion could not be located.[11]

Anion Template Effect. DMSO-d_6 solutions of $1(Y)_4$ (5.0 mM) were heated at 60 °C for 24 h. Interestingly, in the cases of Y$^-$ = PF_6^- and OTf$^-$, no dimerization occurred at all (Scheme 2a). Prolonged heating of the solutions did not induce dimerization. Thermal treatment at 80 °C gave the same results. On the other hand, in the case of Y$^-$ = BF_4^-, similar heating afforded a new species in 7.7% yield.[12] (15.4% of 1^{4+} was converted to the new species.)

The signal pattern of the new species (Figure 4a), which is characterized by 14 independent signals and a large upfield shift of one of the two methylene protons ($\Delta\delta(H_e) = -1.53$ ppm), is similar to that of $2{\supset}(NO_3|NO_3|NO_3)^{5+}$ (Figure 4b). The large upfield shift of H_e in $2{\supset}(NO_3|NO_3|NO_3)^{5+}$ results from a shielding effect, because methylene proton H_e lies on a benzene ring of a neighboring strand of 2^{8+} (Figure 4b, inset). Thus, this upfield shift is one piece of evidence for the interlocked structure. ^{1}H DOSY confirmed that the new species is an interlocked metallohelicate, because its diffusion rate is very similar to that of $2{\supset}(NO_3|NO_3|NO_3)^{5+}$ (Figure S2a in the Supporting Information). The NMR and ESI-MS measurements demonstrate that the new species is $2{\supset}(BF_4|BF_4|BF_4)^{5+}$ (Figure S2 in the Supporting Information). The signals of the encapsulated BF_4^- ions appear at $\delta = -142.9$ and -144.4 ppm with relative signal intensities of 2:1. The signal of free BF_4^- appears at $\delta = -148.3$ ppm, indicative of slow anion exchange on the NMR time scale. The relative position of two interlocked 1^{4+} in $2{\supset}(BF_4|BF_4|BF_4)^{5+}$ is similar to that in $2{\supset}(NO_3|NO_3|NO_3)^{5+}$, because the chemical shifts of H_e−H_i,
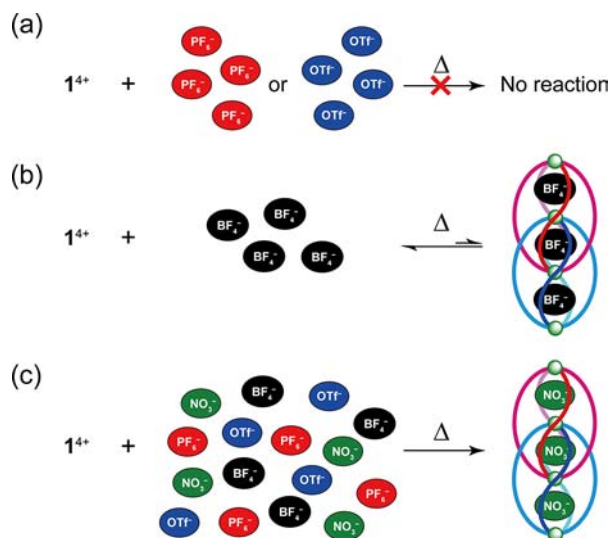
which are susceptible to the relative position of two interlocked 1^{4+}, are very similar to each other. Attempts to crystallize $2{\supset}(BF_4|BF_4|BF_4)^{5+}$ were unsuccessful.

The thermal reaction of $1(BF_4)_4$ at 60 °C for 48 h led to an equilibrium state in which $2{\supset}(BF_4|BF_4|BF_4)^{5+}$ was formed in 9.7% yield (19.4% conversion). No other species, including the 1:1 and 1:2 host−guest complexes of 2^{8+} and BF_4^-, were observed in the ^{1}H and ^{19}F NMR spectra. These results indicate that an equilibrium is established between $2{\supset}(BF_4|BF_4|BF_4)^{5+}$ and monomer and that the equilibrium position lies with monomer (Scheme 2b). This is in contrast to the thermal reaction of 1^{4+} in the presence of NO_3^-, in which the equilibrium position lies far toward $2{\supset}(NO_3|NO_3|NO_3)^{5+}$, as mentioned earlier.[8a] The inability of PF_6^- and OTf$^-$ to induce dimerization and the strong dependency of the equilibrium position on the encapsulated anion demonstrate that the dimerization is driven by the anion template effect.

The fact that the anion templates are essential for the dimerization indicates that the interlocked structure itself is not thermodynamically stable and that the interaction among the bridging ligands of 2^{8+} (C−H···π and π···π interactions, and van der Waals contacts[8a]) alone is insufficient to stabilize the interlocked structure. It is not until 2^{8+} and the three anions form the 1:3 host−guest complex that the interlocked structure is stabilized. This is in contrast with other multi-interlocked systems. For example, the triply interlocked systems reported by Cooper's[7b] and Fujita's[7g] groups do not require auxiliary template species. A similar result was very recently reported by Lindoy's group.[7h] They demonstrated that a triple-stranded helicate undergoes a spontaneous structural conversion to a universal three-ravel structure without an auxiliary template species. In these examples, self-templating stabilizes the entangled structures, and the structural conversion proceeds without requiring auxiliary template species. To understand the detailed mechanism of the dimerization, the origin of the anion template effect was investigated.
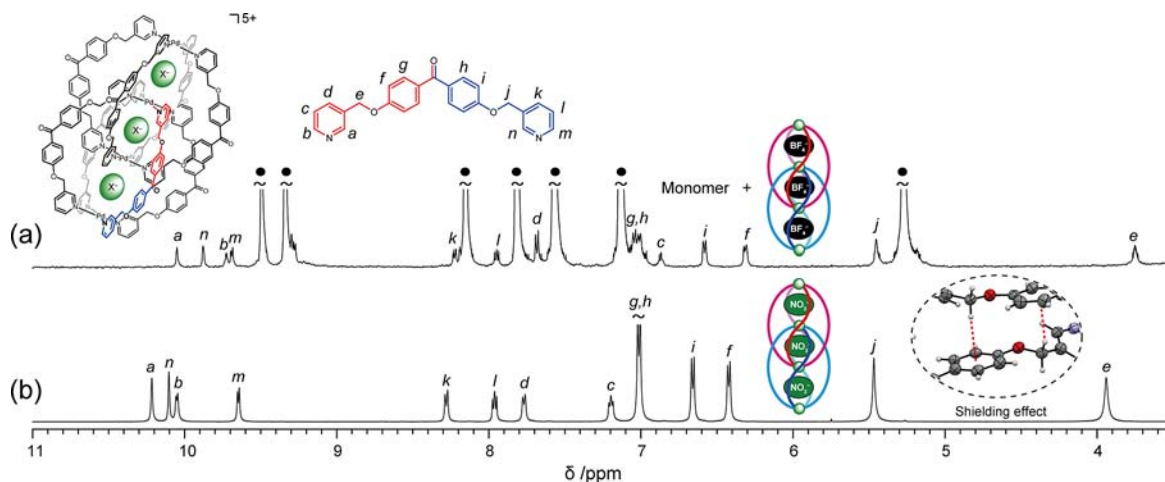
Figure 4. ^{1}H NMR spectra (500 MHz, DMSO-d_6, rt) of (a) an equilibrium mixture of $2 \supset (BF_4|BF_4|BF_4)^{5+}$ and monomer and (b) $2 \supset (NO_3|NO_3|NO_3)^{5+}$. In part a, ● denotes monomer. Monomer = $1 \supset (BF_4)_x^{4-x}$ ($x = 0$–2). The symmetrically independent part of $2 \supset (X|X|X)^{5+}$ is colored with red and blue ($X^- = NO_3^-$, BF_4^-).

Anion Competition Experiment. An anion competition experiment was carried out to investigate the relative affinities of 2^{8+} for NO_3^-, BF_4^-, PF_6^-, and OTf^-. Adding NO_3^-, BF_4^-, PF_6^-, and OTf^- as the tetrabutylammonium (n-Bu)$_4$N$^+$ salts (20.0 mM each) to a DMSO-d_6 solution of $1(BF_4)_4$ (5.0 mM) ($[1^{4+}]:[NO_3^-]:[BF_4^-]:[PF_6^-]:[OTf^-] = 1:4:4:4:4$) followed by heating of the solution at 60 °C for 48 h afforded $2 \supset (NO_3|NO_3|NO_3)^{5+}$ as the sole reaction product (Scheme 2c).[13] ^{19}F NMR spectroscopy confirmed the selective encapsulation of NO_3^-, because the spectrum exhibited only signals of free BF_4^-, PF_6^-, and OTf^- (Figure S3 in Supporting Information). These results demonstrate that (i) 2^{8+} exhibits a much higher affinity for NO_3^- than BF_4^-; (ii) once $2 \supset (NO_3|NO_3|NO_3)^{5+}$ is formed, no anion exchange ($NO_3^- \rightarrow BF_4^-$, PF_6^-, and OTf^-) occurs; and (iii) $2 \supset (NO_3|NO_3|NO_3)^{5+}$ is thermodynamically much more stable than $2 \supset (BF_4|BF_4|BF_4)^{5+}$.

Since $2 \supset (X|X|X)^{5+}$ ($X^- = NO_3^-$, BF_4^-) is a 1:3 host–guest system, the selective anion encapsulation, tight binding, and different thermodynamic stabilities should result from favorable host–guest interactions and the suitable size of NO_3^- as an anion template. The anion recognition properties of 2^{8+} are closely related to those of 1^{4+}, because 2^{8+} consists of two mechanically interlocked 1^{4+}. To clarify these factors, we have investigated (i) the anion recognition properties of 1^{4+} for the three anions (NO_3^-, BF_4^-, and PF_6^-); (ii) the relationship between the cavities of 2^{8+} and the anions in terms of their Rebek's packing coefficients;[14] (iii) the host–guest interaction between 1^{4+} and X^-, as well as between 2^{8+} and X^-, using model host–guest complexes of 1^{4+} and X^- ($1_M \supset (X)$) and 2^{8+} and X^- ($2_M \supset (X)$), respectively; and (iv) the kinetics of the NO_3^--induced dimerization.

i. Anion Recognition. The anion recognition properties of 1^{4+} for NO_3^-, BF_4^-, and PF_6^- were investigated by ^{1}H NMR titration experiments. The experiments were carried out by the addition of 0.5–8 equiv of NO_3^-, BF_4^-, or PF_6^- as the (n-Bu)$_4$N$^+$ salt to a DMSO-d_6 solution of $1(OTf)_4$ (1.0 mM) at room temperature. The ^{1}H NMR spectra were recorded immediately after the addition of the anion. Previously, it was demonstrated that 1^{4+} exhibits a negligible affinity for OTf^-.[8b]

Parts a and b of Figure 5 show the chemical shift changes of H_a and H_b, respectively, upon addition of NO_3^-, BF_4^-, and PF_6^-. 1^{4+} recognizes NO_3^- and BF_4^-, but not PF_6^-. NO_3^- and
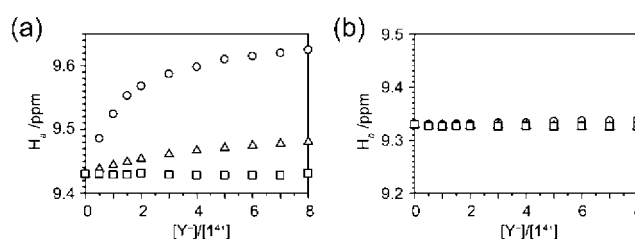

Figure 5. Chemical shift changes of (a) H_a and (b) H_b of 1^{4+} during NMR titrations of NO_3^- (○), BF_4^- (△), and PF_6^- (□).

BF_4^- are encapsulated in the cavity, because only the α-pyridyl proton H_a experienced a downfield shift, probably due to the $C-H_a \cdots O$ (NO_3^-) and $C-H_a \cdots F$ (BF_4^-) hydrogen bonding. Unlike the anions in 2^{8+}, the exchange rate is rapid on the NMR time scale. This rapid exchange is due to the cavity of 1^{4+} being sterically less crowded than that of 2^{8+}, which facilitates the passage of the anion and solvent molecules in and out of the cavity.

The titration experiments were analyzed by a nonlinear least-squares fitting procedure using the WinEQNMR2 program.[15] The titration curves could be best fitted to a 1:2 host-to-guest ratio (Figures S4 and S5 in the Supporting Information). This result is reasonable, because 1^{4+} has the two Pd^{2+} centers. The calculated association constants, $\log_{10}(K_{a1})$ and $\log_{10}(K_a)$, where $K_{a1} = [1 \supset (Y)^{3+}]/\{[1^{4+}][Y^-]\}$, $K_a = [1 \supset (Y)_2^{2+}]/\{[1^{4+}][Y^-]^2\}$, and $Y^- = NO_3^-$ or BF_4^-, are listed in Table 1. As expected, 1^{4+} exhibits a strong affinity for NO_3^- but a weak affinity for BF_4^-. The anion recognition properties of 1^{4+} for the four anions are in good agreement with the coordination

Table 1. Association Constants, $\log_{10}(K_{a1})$, $\log_{10}(K_a)$, and $\log_{10}(K_{a2})$, for the Complexation of Anions by 1^{4+}

anion Y$^-$	$\log_{10}(K_{a1})^a$	$\log_{10}(K_a)^b$	$\log_{10}(K_{a2})^c$
NO_3^-	3.7(2)	5.9(2)	2.2
BF_4^-	2.41(8)	3.6(4)	1.2
OTs^{-d}	2.9(3)	5.1(5)	2.2
ONs^{-d}	3.01(10)	5.57(14)	2.6

$^a K_{a1} = [1 \supset (Y)^{3+}]/\{[1^{4+}][Y^-]\}$. $^b K_a = [1 \supset (Y)_2^{2+}]/\{[1^{4+}][Y^-]^2\}$. $^c K_{a2} = K_{a1}/K_a = [1 \supset (Y)_2^{2+}]/\{[1 \supset (Y)^{3+}][Y^-]\}$. ^{d} Reference 8b.

ability of the anions, i.e., strong (NO_3^-), weak (BF_4^-), and very weak (PF_6^-, OTf$^-$), indicating that not only electrostatic interactions but also the Lewis basicity of the anions affects host−guest complexation. Most likely, the size of the anions is not very important for the host−guest complexation, because the cavity volume of 1^{4+} (ca. 406 Å^3)[8b] is much larger than the anions. In all cases, $\log_{10}(K_{a2})$ ($=\log_{10}(K_a) - \log_{10}(K_{a1})$, $K_{a2} = [\mathbf{1} \supset (Y)_2{}^{2+}]/\{[\mathbf{1} \supset (Y)^{3+}][Y^-]\}$) is smaller than $\log_{10}(K_{a1})$, indicating a negative allosteric effect on the inclusion of the second anion, probably due to electrostatic repulsion between the first and second anions. The titration experiments suggest that the strong affinity of 2^{8+} for NO_3^- originates in part from the strong affinity of 1^{4+} for NO_3^-.

ii. Packing Coefficient. The packing coefficient (PC) is defined as PC = nV_{guest}/V_{cavity}, where n = the number of guests encapsulated in a cavity, V_{guest} = the volume of the guest, and V_{cavity} = the volume of the cavity.[14] Rebek's group demonstrated that a PC of 0.55 ± 0.09 gives the best binding constants for resulting host−guest complexes. The anion volumes[16] of NO_3^-, BF_4^-, and PF_6^- and the PCs of these anions in the cavities of 2^{8+} (ca. 62 Å^3) are listed in Table 2. The PCs demonstrate that

Table 2. Anion Volumes (Å^3) and Packing Coefficients (PCs)

anion	volume /Å^{3a}	PC^b
NO_3^-	34	0.55
BF_4^-	42	0.68
PF_6^-	58	0.94

^{a}Anion volume.[16] ^{b}PC = nV_{guest}/V_{cavity}.[14]

NO_3^- and BF_4^- can be templates for the interlocked structure, whereas PF_6^- cannot, because PF_6^- is too large to be encapsulated in the cavities [PC(PF_6^-) = 0.94]. Plainly, OTf$^-$ is larger than PF_6^- and cannot be a template either. These are consistent with the inability of PF_6^- and OTf$^-$ to induce dimerization. The PCs also indicate that NO_3^- is an ideal template, whereas BF_4^- is not, because its PC is close to Rebek's limiting value (PC ≈ 0.70).

The shape of the anions (NO_3^-, trigonal; BF_4^-, tetrahedral) is not very important. $2 \supset (BF_4|BF_4|BF_4)^{5+}$ and $2 \supset (NO_3|NO_3|NO_3)^{5+}$ adopt an average D_{4h} symmetry on the NMR time scale, irrespective of the symmetries of the encapsulated anions (Figure 4, parts a and b, respectively). These observations indicate that the encapsulated anions are tumbling, rather than being locked in one orientation.

iii. Host−Guest Interaction. Density functional theory (DFT) calculations[17,18] of the model host−guest complexes, $1_M \supset (X)$ and $2_M \supset (X)$, in which anion X$^-$ is placed between two $[Pd(py)_4]^{2+}$ (py = pyridine) units (Figure 6), were carried out.
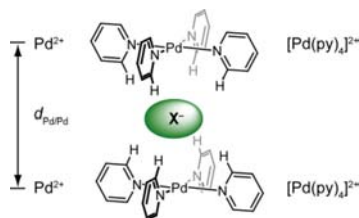

Figure 6. Schematic representation of the model host−guest complex and the definition of $d_{Pd/Pd}$, which is fixed to 16.14 Å for $1_M \supset (X)$ and to 8.32 Å for $2_M \supset (X)$.

The Pd^{2+}/Pd^{2+} separations ($d_{Pd/Pd}$) were fixed to $d_{Pd/Pd}$ = 16.14 Å for $1_M \supset (X)$ and $d_{Pd/Pd}$ = 8.32 Å for $2_M \supset (X)$. These values are the Pd^{2+}/Pd^{2+} separations of the X-ray crystal structures of 1^{4+} (Figure 3) and 2^{8+} (Figure 1),[8a] respectively. The energy-minimized structures were calculated at the B3LYP/6-31G(d,p) level, and the results are shown in Figure S6 in the Supporting Information. In addition, those of $1_M \supset (NO_3)$ and $2_M \supset (NO_3)$ are also shown in parts a and b of Figure 7, respectively. The selected interatomic distances of $1_M \supset (X)$ and $2_M \supset (X)$ are listed in Tables S1 and S2, respectively, in the Supporting Information.
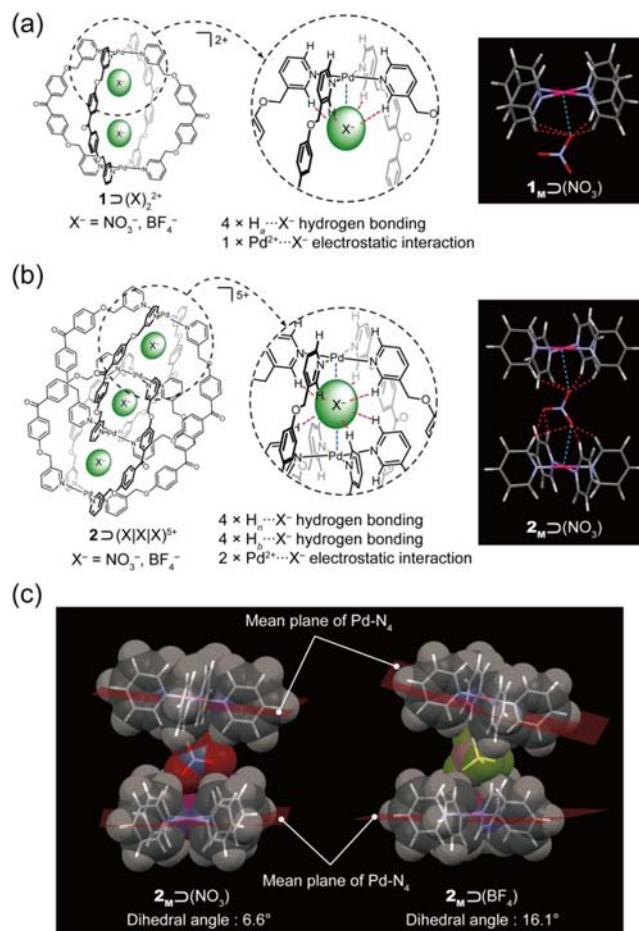

Figure 7. Schematic representation of the environments around the anions (a) in the cavity of 1^{4+} and (b) in cavity A of 2^{8+}. (Right) Energy-minimized (B3LYP/6-31G(d,p)) structures of (a) $1_M \supset (NO_3)$ and (b) $2_M \supset (NO_3)$. In part a, one of the two $[Pd(py)_4]^{2+}$ units remote from the NO_3^- ion is omitted. (c) van der Waals representation of the model host−guest complexes of $2_M \supset (NO_3)$ and $2_M \supset (BF_4)$. Color scheme: gray (carbon), white (hydrogen), orange (boron), blue (nitrogen), red (oxygen), green (fluorine), purple (palladium).

As indicated by the chemical shift of H$_a$ in 1^{4+} in the presence of X$^-$ and those of H$_a$, H$_b$, and H$_n$ in $2 \supset (X|X|X)^{5+}$, the DFT calculations suggest the presence of hydrogen bonding between the α-pyridyl hydrogen atoms and X$^-$. In addition, the oxygen atom of NO_3^- and the fluorine atom of BF_4^- point to the Pd^{2+} center, which may imply an interaction between the lone pair of the anion and the d_{z^2} orbital of the Pd^{2+} center. The Pd^{2+}···O distances are 2.761 Å for $1_M \supset (NO_3)$ and 3.111 and 3.101 Å for $2_M \supset (NO_3)$. The Pd^{2+}···F distances are 2.826 Å for $1_M \supset (BF_4)$ and 3.058 and 3.206 Å for $2_M \supset (BF_4)$. The longer Pd^{2+}···X$^-$

10991

dx.doi.org/10.1021/ja303634u | *J. Am. Chem. Soc.* 2012, 134, 10987−10997

distances in $2_M \supset (X)$ are due to the anion interacting with the upper and lower Pd^{2+} centers at the same time. Interestingly, the dihedral angles between the mean planes defined by the $Pd^{2+}-N_4$ coordination site of $2_M \supset (X)$ are 6.6° ($X^- = NO_3^-$) and 16.1° ($X^- = BF_4^-$) (Figure 7c). The large dihedral angle of $2_M \supset (BF_4)$ results from the larger size of BF_4^- in comparison with NO_3^-.

The enthalpies of host–guest complexation per one anion in the gas phase $[\Delta H(X^-, d_{Pd/Pd})]$ were calculated at the B3LYP/6-311G$^+$(d,p) level, and the results are listed in Table 3. The

Table 3. Enthalpies of Host–Guest Complexation Per One Anion $[\Delta H(X^-, d_{Pd/Pd})]$ in the Gas Phase (B3LYP/6-311G$^+$(d,p) level)

anion X$^-$	$\Delta H(X^-, 16.14\ \text{Å})/\text{kJ mol}^{-1}$	$\Delta H(X^-, 8.32\ \text{Å})/\text{kJ mol}^{-1}$
NO_3^-	−802.3	−1012.8
BF_4^-	−776.7	−992.7

model hosts exhibit a much higher affinity for NO_3^- than BF_4^- in the two different $d_{Pd/Pd}$. For example, in the case of $1_M \supset (X)$, $\Delta H(NO_3^-, 16.14\ \text{Å}) - \Delta H(BF_4^-, 16.14\ \text{Å}) = -25.6\ \text{kJ mol}^{-1}$. These theoretical calculations are in good agreement with the results of the anion competition and the ^1H NMR titration experiments.

Importantly, $|\Delta H(X^-, 8.32\ \text{Å})|$ is considerably larger than $|\Delta H(X^-, 16.14\ \text{Å})|$. That is, the dimerization enhances the host–guest interaction. This enhancement is due to the anion interacting with both the $[Pd(py)_4]^{2+}$ units (Figures 7b and S6c and S6d in the Supporting Information). The observed ^1H NMR spectra support the relationship $|\Delta H(X^-, 8.32\ \text{Å})| \gg |\Delta H(X^-, 16.14\ \text{Å})|$. The signals of H_a, H_b, and H_n of $2 \supset (BF_4|BF_4|BF_4)^{5+}$ and $2 \supset (NO_3|NO_3|NO_3)^{5+}$ appear at a more downfield region (Figure 4a and 4b) compared to those of H_a and H_b of 1^{4+} in the presence of BF_4^- or NO_3^-, indicating that the three anions in $2 \supset (X|X|X)^{5+}$ form stronger hydrogen bonds with the surrounding α-pyridyl hydrogen atoms.

iv. Kinetics. DMSO-d_6 solutions of $1(NO_3)_4$ (2.0 mM) were subjected to heating at given temperatures, and the variations in the concentrations of monomer and $2 \supset (NO_3|NO_3|NO_3)^{5+}$ were examined by ^1H NMR spectroscopy. The plots of $[\text{monomer}]^{-1}$ as a function of reaction time at the different temperatures exhibit a linear relationship (Figure S7 in the Supporting Information), indicating a second-order reaction. That is, the collision of two monomers is the rate-determining step. This result is reasonable, because the host–guest complexation between 1^{4+} and NO_3^- is much faster than the dimerization.[19] No direct formation of $2 \supset (NO_3|NO_3|NO_3)^{5+}$ from the starting materials (Pd^{2+}, L, and NO_3^-) can be explained, because the self-assembly of the 15 components ($4 \times Pd^{2+} + 8 \times L + 3 \times NO_3^-$) to form one supramolecular complex is entropically disfavored. The activation energy for the dimerization is estimated to be +108.9 kJ mol^{-1} by the Arrhenius plot (Table S3 and Figure S8 in the Supporting Information).

Dimerization. The DFT calculations demonstrated that the dimerization enhances the host–guest interaction, and thus, this interaction is the principal driving force of the dimerization. In addition, compared to BF_4^-, NO_3^- strongly stabilizes the interlocked structure $[\Delta H(NO_3^-, 8.32\ \text{Å}) - \Delta H(BF_4^-, 8.32\ \text{Å}) = -20.1\ \text{kJ mol}^{-1}]$. The contribution of the interactions between the bridging ligands of 2^{8+} to the driving force is not

sufficiently large, because no dimerization occurs without a suitable template species, as mentioned earlier.

On the other hand, the dimerization considerably decreases the cavity volume from ca. 406 Å^3 (one big cavity of 1^{4+}) to ca. 62 Å^3 (for each of the three cavities of 2^{8+}). Clearly, the steric complementation between the host cavity and the template is an important factor for the template-directed self-assembly. For example, Fujita's group reported that a tubular supramolecular complex is formed only when an organic carboxylate of a suitable size and shape coexists in solution.[20] In the present case, the size of the anions affects the stability of the interlocked structure due to the anions tumbling in the cavities. From the PC of BF_4^- (Table 2) and the energy-minimized structure of $2_M \supset (BF_4)$ that has the large dihedral angle between the two $Pd-N_4$ sites (Figure 7c), the three BF_4^- ions impose strain on 2^{8+}, whereas the three NO_3^- ions do not, as suggested by the DFT calculation and evidenced by the X-ray crystal structure of 2^{8+} (Figure 1), in which the mean planes of the two $Pd-N_4$ sites are coplanar.

These differences, i.e., the host–guest interaction and the size of the anions, result in the different anion template effects of NO_3^- and BF_4^- and are the origin of the different thermodynamic stabilities of $2 \supset (NO_3|NO_3|NO_3)^{5+}$ and $2 \supset (BF_4|BF_4|BF_4)^{5+}$.

Monomerization Induced by 2-Naphthalenesulfonate. There are several examples of structural interconversions driven by the anion template effect.[21] For example, Lehn et al. reported that anion exchange induces a structural interconversion between pentanuclear and hexanuclear helicates.[21c] These examples demonstrate that even a tiny difference in the nature of the anions may drastically affect the product distribution of the final assemblies. The driving force for these structural interconversions is the stabilization of one particular assembly over another due to favorable interactions between the assembly (host) and the template (guest), and thus, the final assembly represents a minimum in the energy profile of the system based on a combination of enthalpic and entropic factors.[22]

In the present case, the high thermodynamic stability of $2 \supset (NO_3|NO_3|NO_3)^{5+}$ originates from the large enthalpic stabilization of the interlocked structure by the host–guest interaction and the suitability of NO_3^- as the anion template. Thus, if a molecule expels the NO_3^- ion(s) from $2 \supset (NO_3|NO_3|NO_3)^{5+}$, monomerization should occur. In addition, if such a molecule forms a stable host–guest complex with resulting 1^{4+}, dimerization would be obstructed to a certain extent.

Previously, we reported the 1:2 host–guest complex of 1^{4+} and 2-naphthalenesulfonate (ONs^-) in DMSO-d_6 (Figure 8).[8b] ^1H NMR spectroscopy and X-ray diffraction analysis revealed that the sulfonate group of ONs^- exhibits a relatively high affinity for the Pd^{2+} centers due to $Pd^{2+} \cdots O_3 SR^-$ interaction and $C-H_a \cdots O_3 SR^-$ hydrogen bonding. These interactions encourage host–guest complexation with relatively high association constants (Table 1). Thus, it was expected that ONs^- may expel the NO_3^- ion(s) from $2 \supset (NO_3|NO_3|NO_3)^{5+}$ through anion exchange. In addition, this anion alone cannot induce dimerization.[8b] On the basis of these backgrounds, we have attempted monomerization of $2 \supset (NO_3|NO_3|NO_3)^{5+}$ with ONs^-.

The thermal reaction of $[2 \supset (NO_3|NO_3|NO_3)](NO_3)_5$ (2.0 mM) with 8 equiv of ONs^- as a sodium salt in DMSO-d_6 at 60 °C was carried out ($[2 \supset (NO_3|NO_3|NO_3)^{5+}]:[NO_3^-]:[ONs^-]$ = 1:5:8, reaction condition I). As expected, monomerization
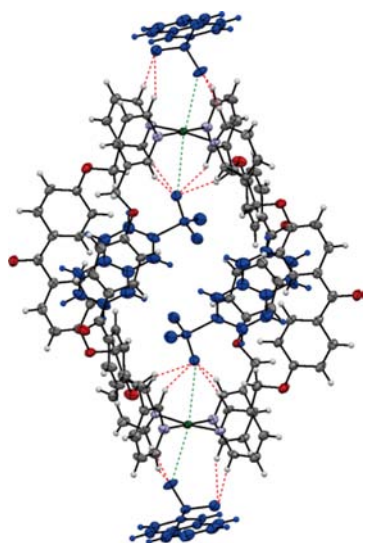
Figure 8. ORTEP drawing of the X-ray crystal structure of $[1{\supset}(ONs)_2](ONs)_2$ (50% probability ellipsoids).[8b] In the solid-state, the Pd^{2+} centers form pseudo-octahedral coordination geometry due to the occupancy of the axial positions by the oxygen atoms of the ONs^- ions. Color scheme: gray (carbon), white (hydrogen), light-blue (nitrogen), red (oxygen), green (palladium), blue (ONs^-). Green and red dotted lines denote $Pd^{2+}{\cdots}O_3SR^-$ interaction and $C-H{\cdots}O_3SR^-$ hydrogen bonding, respectively.

occurred. The equilibrium was established after ca. 72 h, and the reaction afforded monomer in 28.0% yield[12] (14.0% of $2{\supset}(NO_3|NO_3|NO_3)^{5+}$ was monomerized). Interestingly, a trace amount of a new species was detected. To promote monomerization, a thermal reaction under a higher concentration of ONs^- (24 equiv) was carried out ($[2{\supset}(NO_3|NO_3|NO_3)^{5+}]$:$[NO_3^-]$:$[ONs^-]$ = 1:5:24, reaction condition II). Again, the solution contained only $2{\supset}(NO_3|NO_3|NO_3)^{5+}$, monomer, and the new species throughout the reaction (Figures 9 and S9 in the Supporting Information). This new species is neither a 1:1 nor a 1:2 host–guest complex of 2^{8+} and NO_3^- and is not the host–guest complex of 1^{4+} and ONs^-, because none of these host–guest complexes were observed in the previous studies.[8] No monomerization occurred when naphthalene was used instead of ONs^-, indicating that the affinity of the sulfonate group for the Pd^{2+} center plays a crucial rule in the monomerization.

The signal pattern of the new species, which is characterized by the splitting of the signals of the bridging ligand, is very similar to those of $2{\supset}(NO_3|NO_3|NO_3)^{5+}$ and $2{\supset}(BF_4|BF_4|BF_4)^{5+}$. ^{1}H-DOSY confirmed that this species is an interlocked

metallohelicate, because its diffusion rate is very similar to that of coexisting $2{\supset}(NO_3|NO_3|NO_3)^{5+}$ (Figure S10a in the Supporting Information). The NMR and ESI-MS measurements indicate that the new species is $2{\supset}(ONs|NO_3|ONs)^{5+}$, where the sulfonate groups of ONs^- are encapsulated in cavities A (Figure S10b−d in the Supporting Information). In $2{\supset}(ONs|NO_3|ONs)^{5+}$, two interlocked 1^{4+} slide apart to expand cavities A to encapsulate the sulfonate group of ONs^-, while at the same time, cavity B contracts, and the NO_3^- ion is encapsulated more tightly $[\Delta\delta(H_a) = +1.46$ ppm$]$, resulting in a weakened shielding effect $[\Delta\delta(H_e) = +0.76$ ppm$]$ (Figure 9). An attempt to crystallize $2{\supset}(ONs|NO_3|ONs)$ was unsuccessful.

The host–guest complexation between 1^{4+} and ONs^- was confirmed by the characteristic downfield shift of the signal of H_a in 1^{4+} $[\Delta\delta(H_a) = +0.66$ ppm$]$, compared to the signal of H_a of 1^{4+} in the presence of NO_3^- alone].[8b] This downfield shift is due to $C-H_a{\cdots}O_3SR^-$ hydrogen bonding. In addition, in contrast to the thermal decomposition of $2{\supset}(NO_3|NO_3|NO_3)^{5+}$, in which the resulting monomers almost completely converted back into $2{\supset}(NO_3|NO_3|NO_3)^{5+}$,[8a] the product distribution remained unchanged at room temperature, indicating that the host–guest complexation between 1^{4+} and ONs^- obstructs the dimerization.

Intermediate. Figure 10 shows the time course of the product distribution of $2{\supset}(NO_3|NO_3|NO_3)^{5+}$, monomer, and
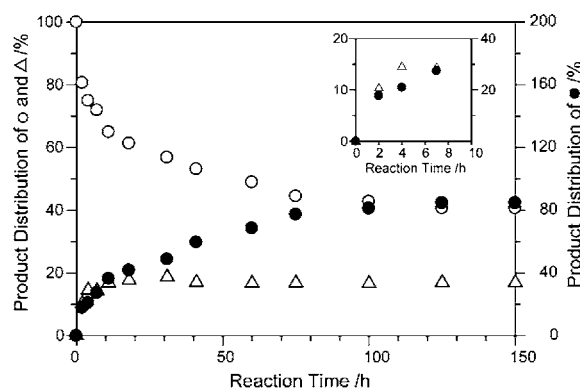

Figure 10. Time course of the thermal reaction of $[2{\supset}(NO_3|NO_3|NO_3)](NO_3)_5$ (2.0 mM) with ONs^- as sodium salt (48.0 mM). O, ●, and △ denote $2{\supset}(NO_3|NO_3|NO_3)^{5+}$, monomer, and $2{\supset}(ONs|NO_3|ONs)^{5+}$, respectively. Monomer = $1{\supset}(NO_3)_x(ONs)_y^{4-(x+y)}$ ($x + y$ = 0−2).

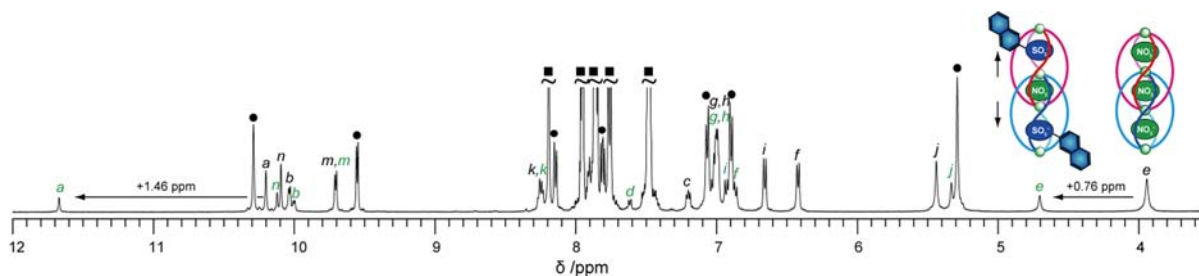$2{\supset}(ONs|NO_3|ONs)^{5+}$. The reaction reached an equilibrium state after ca. 125 h, at which the product distribution of

Figure 9. ^{1}H NMR spectrum (500 MHz, DMSO-d_6, rt) of an equilibrium mixture of $2{\supset}(NO_3|NO_3|NO_3)^{5+}$ (black), monomer, and the new species ($2{\supset}(ONs|NO_3|ONs)^{5+}$, green) (reaction condition II). ● and ■ denote monomer and ONs^-, respectively. Monomer = $1{\supset}(NO_3)_x(ONs)_y^{4-(x+y)}$ ($x + y$ = 0−2).

Scheme 3. Equilibrium among the Three Supramolecular Complexes $2 \supset (NO_3|NO_3|NO_3)^{5+}$, Monomer $[1 \supset (NO_3)_x(ONs)_y^{4-(x+y)}$ ($x + y = 0-2$)], and $2 \supset (ONs|NO_3|ONs)^{5+}$
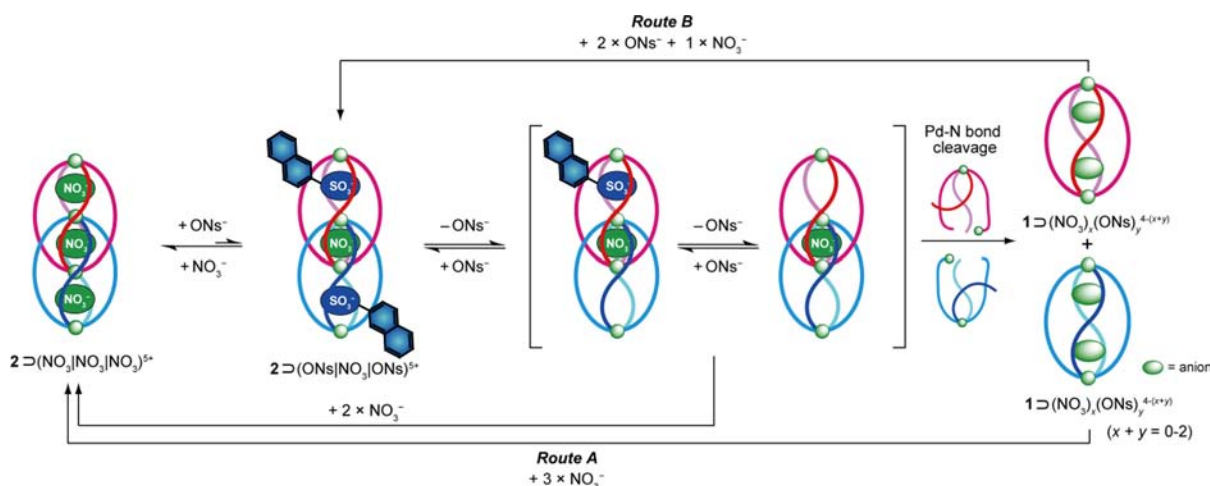
$2 \supset (NO_3|NO_3|NO_3)^{5+}$, monomer, and $2 \supset (ONs|NO_3|ONs)^{5+}$ was 40.7%, 84.6% and 17.0%, respectively[12] (42.3% and 17.0% of $2 \supset (NO_3|NO_3|NO_3)^{5+}$ was converted to monomer and $2 \supset (ONs|NO_3|ONs)^{5+}$, respectively). Figure 10 (inset) shows that $2 \supset (ONs|NO_3|ONs)^{5+}$ increased immediately, followed by an increase in monomer. For example, at a reaction time of 4 h, 10.5% and 14.6% of $2 \supset (NO_3|NO_3|NO_3)^{5+}$ was converted to monomer and $2 \supset (ONs|NO_3|ONs)^{5+}$, respectively. After ca. 10 h, the concentration of $2 \supset (ONs|NO_3|ONs)^{5+}$ reached a plateau (17%−18%), suggesting that $2 \supset (ONs|NO_3|ONs)^{5+}$ is an intermediate and that an equilibrium was established among the three supramolecular complexes. This assumption is supported by the thermal reaction of $[1 \supset (ONs)_2](ONs)_2$ (1.0 mM) with a low concentration of NO_3^- as the (n-Bu)$_4$N$^+$ salt (0.5 mM) in DMSO-d_6 at 60 °C. The reaction afforded $2 \supset (ONs|NO_3|ONs)^{5+}$ as the sole reaction product (Figure S11 in the Supporting Information).

Structural Interconversion. Scheme 3 shows the equilibrium among $2 \supset (NO_3|NO_3|NO_3)^{5+}$, monomer, and $2 \supset (ONs|NO_3|ONs)^{5+}$. Under the reaction condition II ($[2 \supset (NO_3|NO_3|NO_3)^{5+}]:[NO_3^-]:[ONs^-] = 1:5:24$), 40.7% of $2 \supset (NO_3|NO_3|NO_3)^{5+}$ still exists at the thermal equilibrium, despite the presence of an excess amount of ONs^-. This result indicates that 2^{8+} exhibits a higher affinity for NO_3^- than ONs^-. Therefore, the equilibrium position of the eq 1 lies to the left side.
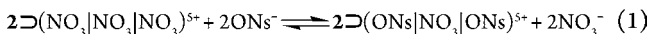
$$2 \supset (NO_3|NO_3|NO_3)^{5+} + 2ONs^- \rightleftharpoons 2 \supset (ONs|NO_3|ONs)^{5+} + 2NO_3^- \quad (1)$$

Figure 9 shows that $2 \supset (ONs|NO_3|ONs)^{5+}$ adopts an average D_{4h} symmetry on the NMR time scale and that there is only one set of the signals of ONs^-, indicating rapid anion exchange (ONs^- in 2^{8+} ↔ free ONs^- ↔ ONs^- in 1^{4+}) on the NMR time scale. Because the anion templates are essential for sustaining the interlocked structure, the dissociation of ONs^- from $2 \supset (ONs|NO_3|ONs)^{5+}$ destabilizes the interlocked structure. Therefore, the resulting unstable complexes monomerize via the Pd^{2+}−N bond cleavage or capture ONs^- or NO_3^- to go back to $2 \supset (ONs|NO_3|ONs)^{5+}$ or convert to $2 \supset (NO_3|NO_3|NO_3)^{5+}$, respectively (Scheme 3).

Whether resulting 1^{4+} dimerizes depends on the relative concentrations of NO_3^- and ONs^-. These anions compete with

each other for the host−guest complexation with 1^{4+}. Therefore, the following equilibrium is established in solution:

In the case of $[NO_3^-] \approx [ONs^-]$, the equilibrium position of eq 2 lies to the left side, because 1^{4+} exhibits a higher affinity for

$$(2)$$
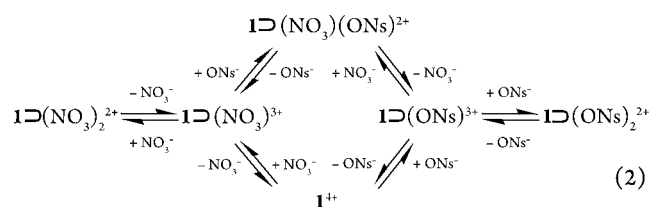
NO_3^- than ONs^- (Table 1), and the dimerization proceeds mainly via route A, in which two 1^{4+} and three NO_3^- ions afford $2 \supset (NO_3|NO_3|NO_3)^{5+}$ (Scheme 3). With increasing the concentration of ONs^-, the equilibrium position shifts toward the middle to the right side, and route B, in which two 1^{4+}, two ONs^- ions, and one NO_3^- ion afford $2 \supset (ONs|NO_3|ONs)^{5+}$, begins to compete with route A. In the case of $[NO_3^-] \ll [ONs^-]$, the dimerization is to a large extent obstructed by the formation of $1 \supset (ONs)_2$.

The product distribution at the thermal equilibrium under the given reaction conditions can be explained as follows. Under the reaction condition I ($[2 \supset (NO_3|NO_3|NO_3)^{5+}]:[NO_3^-]:[ONs^-] = 1:5:8$), only 14.0% of $2 \supset (NO_3|NO_3|NO_3)^{5+}$ was monomerized, and a trace amount of $2 \supset (ONs|NO_3|ONs)^{5+}$ was formed. This result is because under the given reaction conditions, the anion exchange on $2 \supset (NO_3|NO_3|NO_3)^{5+}$ proceeds slightly, and 1^{4+} dimerizes mainly via route A. Under the reaction condition II, 42.3% of $2 \supset (NO_3|NO_3|NO_3)^{5+}$ was monomerized and 17.0% of $2 \supset (ONs|NO_3|ONs)^{5+}$ coexisted in the solution. This occurs because under the high ONs^- concentration, the probability of the anion exchange on $2 \supset (NO_3|NO_3|NO_3)^{5+}$ becomes high and monomerization proceeds efficiently, route B competes with route A, and the dimerization is to a large extent obstructed by the formation of $1 \supset (ONs)_2$.

Solid−Solute Equilibrium. Although ONs^- induces monomerization, both $2 \supset (NO_3|NO_3|NO_3)^{5+}$ and monomer still coexist in the solution. Finally, we have attempted to physically separate $2 \supset (NO_3|NO_3|NO_3)^{5+}$ and monomer.

Previously, we reported that the host−guest complexation of 1^{4+} and p-toluenesulfonate (OTs^-) affords the barely soluble precipitate $[1 \supset (OTs)_2](OTs)_2$.[8b] Because OTs^- also exhibits a relatively high affinity for 1^{4+} (Table 1), it was expected that OTs^- would also induce the monomerization of $2 \supset (NO_3|NO_3|NO_3)^{5+}$, and resulting 1^{4+} and OTs^- would then associate together to form the precipitate $[1 \supset (OTs)_2](OTs)_2$.

Adding 8.2 equiv of OTs^- as the $(n\text{-Bu})_4N^+$ salt to a DMSO-d_6 solution of $[2 \supset (NO_3|NO_3|NO_3)](NO_3)_5$ (2.7 mM) $([2 \supset (NO_3|NO_3|NO_3)^{5+}]:[NO_3^-]:[OTs^-] = 1:5:8.2)$ followed by stirring at 60 °C yielded the white precipitate $[1 \supset (OTs)_2]$-$(OTs)_2$. After heating for 96 h, the reaction reached an equilibrium state (Figure 11). The product distribution was
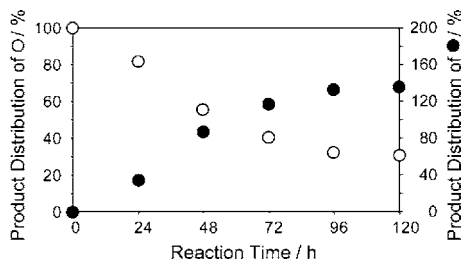

Figure 11. Time course of the thermal reaction of $[2 \supset (NO_3|NO_3|NO_3)](NO_3)_5$ (2.7 mM) with OTs^- as the $(n\text{-Bu})_4N^+$ salt (22.1 mM). ● and ○ denote monomer and $2 \supset (NO_3|NO_3|NO_3)^{5+}$, respectively. Monomer = $1 \supset (OTs)_x^{4-x}$ $(x = 0-2)$.

determined by integrating the signals of $2 \supset (NO_3|NO_3|NO_3)^{5+}$ and $(n\text{-Bu})_4N^+$.[23] The proportion of $[1 \supset (OTs)_2](OTs)_2$ (precipitate) and $2 \supset (NO_3|NO_3|NO_3)^{5+}$ (solute) at the thermal equilibrium was 136% and 32%, respectively. This result indicates that 68% of $2 \supset (NO_3|NO_3|NO_3)^{5+}$ monomerized. Intermediate $2 \supset (OTs|NO_3|OTs)^{5+}$ was not detected due to $[NO_3^-] > [OTs^-]$ in the solution.[24] The ^1H NMR spectra of

the solution at the equilibrium state and of the precipitate dissolved in DMSO-d_6 (suspension) are shown in parts a and b of Figure 12, respectively. The solution contained $2 \supset (NO_3|NO_3|NO_3)^{5+}$ and a trace amount of monomer, while the suspension contained only monomer and there are none of the signals of $(n\text{-Bu})_4N^+$. These results indicate that OTs^- induces monomerization and the formation of the precipitate $[1 \supset (OTs)_2](OTs)_2$, whereas a slight amount of $[1 \supset (OTs)_2]$-$(OTs)_2$ dissolves in the solution and dimerizes to give $2 \supset (NO_3|NO_3|NO_3)^{5+}$ via anion exchange. Apparently, OTs^- promotes monomerization more efficiently than ONs^-. However, this is due to the barely soluble nature of $[1 \supset (OTs)_2](OTs)_2$. That is, the precipitation promotes monomerization due to Le Chatelier's principle. Because of this behavior, we could accomplish the physical separation of the monomer and the interlocked metallohelicate.

■ CONCLUSIONS

We have demonstrated that the dimerization of 1^{4+} is driven by the anion template effect. The thermodynamic stability of $2 \supset (X|X|X)^{5+}$ strongly depends on the encapsulated three anions X^- $(X^- = NO_3^-, BF_4^-)$. In the case of $X^- = NO_3^-$, the equilibrium position lies far toward $2 \supset (NO_3|NO_3|NO_3)^{5+}$, and monomerization is difficult, whereas in the case of $X^- = BF_4^-$, the equilibrium position lies toward monomer, and only a small amount of $2 \supset (BF_4|BF_4|BF_4)^{5+}$ is formed at the thermal equilibrium state. The experimental results, Rebek's packing coefficients (PCs), and DFT calculations all support the proposal that the difference in the thermodynamic stability originates from both the host−guest interaction between 2^{8+} and X^- and the size of the anion. The high affinity of 2^{8+} for NO_3^- and the ideal size of NO_3^- as an anion template (PC = 0.55) significantly stabilize the interlocked structure and prevent monomerization, while the weak affinity of 2^{8+} for BF_4^- and its large anion size (PC = 0.68) cannot. The inability
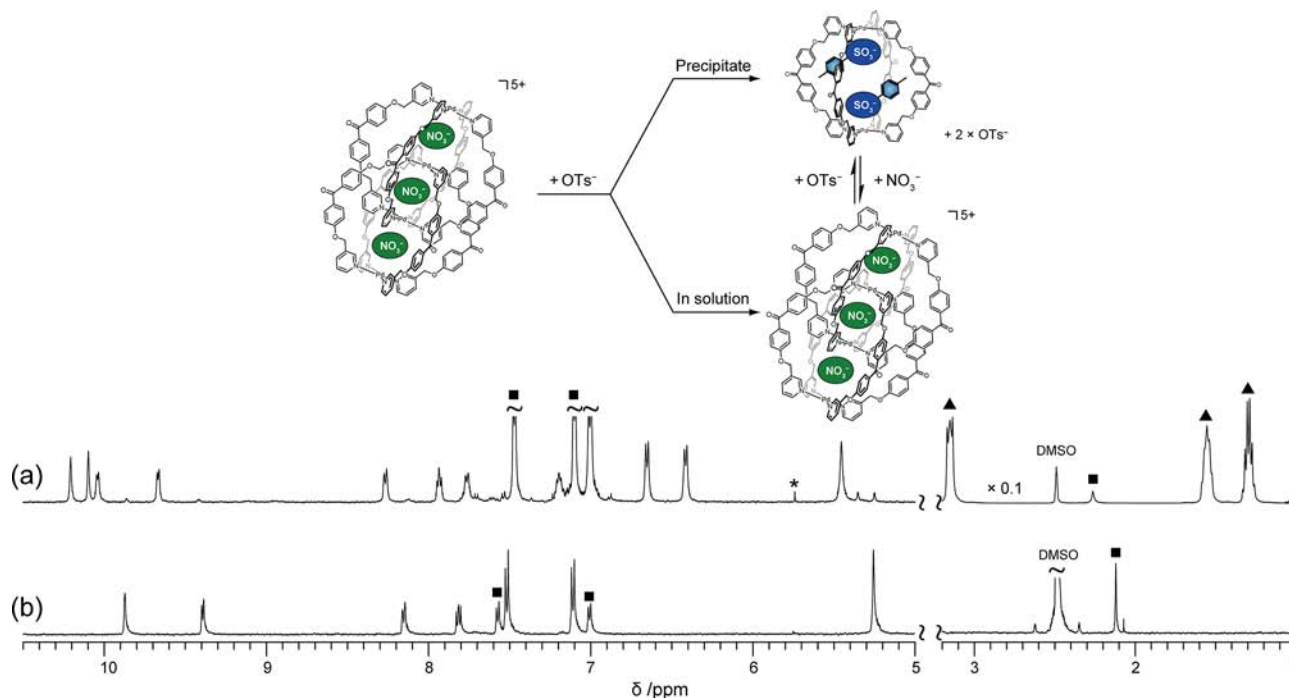

Figure 12. ^1H NMR spectra (500 MHz, DMSO-d_6, rt) of (a) the reaction solution at the equilibrium state and (b) a suspension of $[1 \supset (OTs)_2](OTs)_2$. ■, ▲, and * denote OTs^-, $(n\text{-Bu})_4N^+$, and an impurity (CH_2Cl_2), respectively.

of PF_6^- and OTf^- to induce dimerization results from their size being much larger than those of NO_3^- and BF_4^-, and thus, they cannot be templates of the interlocked structure. These results indicate that, unlike other multi-interlocked systems, such as Cooper's and Fujita's triply interlocked systems, the interlocked structure itself is not thermodynamically stable, and the interaction between the bridging ligands of 2^{8+} alone is insufficient to sustain the interlocked structure. It is not until 2^{8+} and three anions X^- form 1:3 host–guest complex $2 \supset (X|X|X)^{5+}$ that the interlocked structure is stabilized.

We have found that 2-naphthalenesulfonate (ONs^-) induces the monomerization of $2 \supset (NO_3|NO_3|NO_3)^{5+}$ at a lower reaction temperature and obstructs the dimerization of resulting 1^{4+} through the host–guest complexation between 1^{4+} and ONs^-. Detailed investigation has revealed that the important step in the monomerization is the substitution of the NO_3^- ions in cavities A with the sulfonate groups of the ONs^- ions, which affords intermediate $2 \supset (ONs|NO_3|ONs)^{5+}$. The dissociation of the ONs^- ion(s) from the intermediate destabilizes the interlocked structure, because the three anions are required to sustain it. The resulting unstable complexes monomerize or capture ONs^- or NO_3^- to go back to $2 \supset (ONs|NO_3|ONs)^{5+}$ or convert to $2 \supset (NO_3|NO_3|NO_3)^{5+}$, respectively. On the basis of this finding, and using p-toluenesulfonate (OTs^-), the physical separation of $2 \supset (NO_3|NO_3|NO_3)^{5+}$ and 1^{4+} as OTs^- salt was achieved. The results, i.e., the anion-directed formation and degradation of the interlocked structure, may be applicable to the construction of supramolecular switches.

It is also very interesting to note that the relative position of two interlocked 1^{4+} changes when anions of different sizes $(NO_3^-$ and the sulfonate group of $ONs^-)$ are encapsulated. This change implies that 2^{8+} may encapsulate different anions at the same time and may encapsulate other anions whose sizes are similar to or smaller than those of NO_3^- and BF_4^-. Additionally, since the steric environment of cavity A and cavity B is quite different (cavity A is surrounded by the four bridging ligands, whereas cavity B by the eight bridging ligands), this difference may affect the anion recognition properties of 2^{8+}. We are currently investigating the detailed anion recognition properties of 2^{8+} and also performing the design and synthesis of new quadruply interlocked architectures, as well as the applicability of the present interlocked system for use in the preparation of supramolecular polymers.

ASSOCIATED CONTENT

Supporting Information

Material and instruments, X-ray crystallography, experimental procedure, supporting figures and tables, and X-ray crystallographic data of $1(OTf)_4$ (cif). This material is available free of charge via the Internet at http://pubs.acs.org

AUTHOR INFORMATION

Corresponding Author

csekiya@mail.ecc.u-tokyo.ac.jp; ckuroda@mail.ecc.u-tokyo.ac.jp

Present Addresses

§College of Pharmaceutical Sciences, Ritsumeikan University, Kusatsu, Shiga 525-8577, Japan, csekiya@fc.ritsumei.ac.jp.
⊥Research Institute for Science and Technology, Tokyo University of Science, 2641 Yamazaki, Noda, Chiba 278-8510, Japan. TEL: +81-4-7122-9619, rkuroda@rs.tus.ac.jp.

Notes

The authors declare no competing financial interest.

REFERENCES

(1) (a) Coskun, A.; Banaszak, M.; Astumian, R. D.; Stoddart, J. F.; Grzybowski, B. A. *Chem. Soc. Rev.* **2012**, *41*, 19−30. (b) Beves, J. E.; Blight, B. A.; Campbell, C. J.; Leigh, D. A.; McBurnery, R. T. *Angew. Chem., Int. Ed.* **2011**, *50*, 9260−9327. (c) Fang., L.; Olson, M. A.; Benítez, D.; Tkatchouk, E.; Goddard, W. A., III; Stoddart, J. F. *Chem. Soc. Rev.* **2010**, *39*, 17−29. (d) Chichak, K. S.; Cantrill, S. J.; Pease, A. R.; Chiu, S.-H.; Cave, G. W. V.; Atwood, J. L.; Stoddart, J. F. *Science* **2004**, *304*, 1308−1312. (e) Breault, G. A.; Hunter, C. A.; Mayers, P. C. *Tetrahedron* **1999**, *55*, 5265−5293. (f) Vögtlet, F.; Safarowsky, O.; Heim, C.; Affeld, A.; Braun, O.; Mohry, A. *Pure Appl. Chem.* **1999**, *71*, 247−251. (g) Fujita, M.; Ogura, K. *Bull. Chem. Soc. Jpn.* **1996**, *69*, 1471−1482. (h) Amabilino, D. B.; Stoddart, J. F. *Chem. Rev.* **1995**, *95*, 2725−2828. (i) Sauvage, J.-P. *Acc. Chem. Res.* **1990**, *23*, 319−327. (j) Buchecker, C. O. D.; Sauvage, J.-P. *Chem. Rev.* **1987**, *87*, 795−810.
(2) (a) Balzani, V.; Credi, A.; Silvi, S.; Venturi, M. *Chem. Soc. Rev.* **2006**, *35*, 1135−1140. (b) Dietrich-Buchecker, C.; Jimenez-Molero, M. C.; Sartor, V.; Sauvage, J.-P. *Pure Appl. Chem.* **2003**, *75*, 1383−1393. (c) Pease, A. R.; Jeppesen, J. O.; Stoddart, J. F.; Luo, Y.; Collier, C. P.; Heath, J. R. *Acc. Chem. Res.* **2001**, *34*, 433−444.
(3) Recent examples: (a) Lu, J.; Turner, D. R.; Harding, L. P.; Byrne, L. T.; Baker, M. V.; Batten, S. T. *J. Am. Chem. Soc.* **2009**, *131*, 10372−10373. (b) Megiatto, J. D.; Schuster, D. I. *J. Am. Chem. Soc.* **2008**, *130*, 12872−12873. (c) Goldup, S. M.; Leigh, D. A.; Lusby, P. J.; McBurnery, R. T.; Slawin, A. M. Z. *Angew. Chem., Int. Ed.* **2008**, *47*, 6999−7003. (d) Blight, B. A.; Wisner, J. A.; Jennings, M. C. *Angew. Chem., Int. Ed.* **2007**, *46*, 2835−2838. (e) Frey, J.; Kraus, T.; Heitz, V.; Sauvage, J.-P. *Chem.—Eur. J.* **2007**, *13*, 7584−7594. (f) Fuller, A.-M.; Leigh, D. A.; Lusbym, P. J. *Angew. Chem., Int. Ed.* **2007**, *46*, 5015−5019. (g) Abedin, T. S. M.; Thompson, L. K.; Miller, D. O. *Chem. Commun.* **2005**, 5512−5514. (h) Hogg, L.; Leigh, D. A.; Lusby, P. J.; Morelli, A.; Parsons, S.; Wong, J. K. Y. *Angew. Chem., Int. Ed.* **2004**, *43*, 1218−1221. (i) Hamann, C.; Kern, J.-M.; Sauvage, J.-P. *Inorg. Chem.* **2003**, *42*, 1877−1883. (j) McArdle, C. P.; Vittal, J. J.; Puddephatt, R. J. *Angew. Chem., Int. Ed.* **2000**, *39*, 3819−3822.
(4) (a) Vilar, R. *Angew. Chem., Int. Ed.* **2003**, *42*, 1460−1477. (b) Cheng, S.−T; Doxiadi, E.; Vilar, R.; White, A. J. P.; Williams, D. J. *J. Chem. Soc., Dalton Trans.* **2001**, 2239−2244. (c) Beer, P. D.; Gale, P. A. *Angew. Chem., Int. Ed.* **2001**, *40*, 486−516.
(5) Recent examples: (a) Li, Y.; Mullen, K, M.; Claridge, T. D. W.; Costa, P. J.; Felix, V.; Beer, P. D. *Chem. Commun.* **2009**, 7134−7136. (b) Campos-Fernández, C. S.; Clérac, R.; Koomen, J. M.; Russell, D. H.; Dunbar, K. R. *J. Am. Chem. Soc.* **2001**, *123*, 773−774. (c) Campos-Fernández, C. S.; Clérac, R.; Dunbar, K. R. *Angew. Chem., Int. Ed.* **1999**, *38*, 3477−3479. (d) Vickers, M. S.; Beer, P. D. *Chem. Soc. Rev.* **2007**, *36*, 211−225. (e) Lankshear, M. D.; Evans, N. H.; Bayly, S. R.; Beer, P. D. *Chem.—Eur. J.* **2007**, *13*, 3861−3870. (f) Bayly, S. R.; Gray, T. M.; Chemielewskim, M. J.; Davis, J. J.; Beer, P. D. *Chem. Commun.* **2007**, 2234−2236. (g) Lankshear, M. D.; Beer, P. D. *Acc. Chem. Res.* **2007**, *40*, 657−668. (h) Ng, K.−Y.; Cowley, A. R.; Beer, P. D. *Chem. Commun.* **2006**, 3676−3678. (i) Beer, P. D.; Sambrook, M. R.; Curiel, D. *Chem. Commun.* **2006**, 2105−2117. (j) Sambrook, M. R.; Beer, P. D.; Wisner, J. A.; Paul, R.; Cowley, A. R. *J. Am. Chem. Soc.* **2004**, *126*, 15364−15365. (k) Ghosh, P.; Mermagen., O.; Schalley, C. A. *Chem. Commun.* **2002**, 2628−2629. (l) Wisner, J. A.; Beer, P. D.; Berry, N. G.; Tomapatanaget, B. *Proc. Natl. Acad. Sci. U. S. A.* **2002**, *99*, 4983−4986. (m) Wisner, J. A.; Beer, P. D.; Drew, M. G. B. *Angew. Chem., Int. Ed.* **2001**, *40*, 3606−3609. (n) Hübner, G. M.; Gläser, J.; Seel, C.; Vögtle, F. *Angew. Chem., Int. Ed.* **1999**, *38*, 383−86. (o) Gong., H. −Y.;

Rambo, B. M.; Karnas, E.; Lynch, V. M.; Sessler, J. L. *J. Am. Chem. Soc.* **2011**, *133*, 1526–1533. (p) Gong, H.-Y.; Rambo, B. M.; Karnas, E.; Lynch, V. M.; Sessler, J. L. *Nat. Chem.* **2010**, *2*, 406–409.

(6) Fujita, M.; Ibukuro, H.; Hagihara, H.; Ogura, K. *Nature* **1994**, *367*, 720–723.

(7) Examples of the triply and quadruply interlocked molecular architectures: (a) Henkelis, J. J.; Ronson, T. K.; Harding, L. P.; Hardie, M. *J. Chem. Commun.* **2011**, *47*, 6560–6562. (b) Hasell, T.; Wu, X.; Jones, T. A.; Basca, J.; Steiner, A.; Mitra, T; Trewin, A.; Adams, D. J.; Cooper, A. I. *Nat. Chem.* **2010**, *2*, 750–755. (c) Ronson, T. K.; Fisher, J.; Harding, L. P.; Rizkallah, P. J.; Warren, J. E.; Hardie, M. J. *Nat. Chem.* **2009**, *1*, 212–216. (d) Yamauchi, Y.; Yoshizawa, M.; Fujita, M. *J. Am. Chem. Soc.* **2008**, *130*, 5832–5833. (e) Westcott, A.; Fisher, J.; Harding, L. P.; Rizkallah, P.; Hardie, M. J. *J. Am. Chem. Soc.* **2008**, *130*, 2950–2951. (f) Wang, L.; Vysotsky, M. O.; Bogdan, A.; Bolte, M.; Böhmer, V. *Science* **2004**, *304*, 1312–1314. (g) Fujita, M.; Fujita, K.; Ogura, K.; Yamaguchi, K. *Nature* **1999**, *400*, 52–55. (h) Jack, F.; Clegg, J. K.; Lindoy, L. F.; Macquart, R. B.; Meehan, G. V. *Nat. Commun.* **2011**, *2*, 205. (i) Freye, S.; Hey, J.; Torras-Galán, A.; Stalke, D.; Herbsy-Irmer, R.; John, M.; Clever, G. H. *Angew. Chem., Int. Ed.* **2012**, *51*, 2191–2194.

(8) (a) Fukuda, M.; Sekiya, R.; Kuroda, R. *Angew. Chem., Int. Ed.* **2008**, *47*, 706–710. (b) Sekiya, R.; Kuroda, R. *Chem. Commun.* **2011**, *47*, 12346–12348.

(9) The volumes of cavities A and B were estimated by *PLATON* program using the X-ray crystal structure data of 2^{8+} (see ref 8a): Spek, A. L. *PLATON*; University of Glasgow: Glasgow, Scotland, 1998.

(10) The quality of the diffraction data was not very good due to the low quality of the single crystal.

(11) None of the guest molecules including OTf⁻ in channel A could be located. This is partly because of the low quality of the diffraction data and partly because of the disorder of the guest molecules in channel A.

(12) Product distribution was determined by ¹H NMR spectroscopy.

(13) The initial solution of **1**(BF$_4$)$_4$ contained only monomer.

(14) Mecozzi, S.; Rebek, J., Jr. *Chem.—Eur. J.* **1998**, *4*, 1016–1022.

(15) Hynes, M. J. *J. Chem. Soc., Dalton Trans.* **1993**, 311–312.

(16) Hayashida, O.; Shivanyuk, A.; Rebek, J., Jr. *Angew. Chem., Int. Ed.* **2002**, *41*, 3423–3426.

(17) (a) Becke, A. D. *J. Chem. Phys.* **1993**, *98*, 5648–5652. (b) Lee, C.; Yang, W.; Parr, R. G. *Phys. Rev. B* **1988**, *37*, 785–789. (c) Vosko, S. H.; Wilk, L.; Nusair, M. *Can. J. Phys.* **1980**, *58*, 1200–1211. (d) Stephens, P. J.; Devlin, F. J.; Chabalowski, C. F.; Frisch, M. J. *J. Phys. Chem.* **1994**, *98*, 11623–11627.

(18) Frisch, M. J.; Trucks, G. W.; Schlegel, H. B.; Scuseria, G. E.; Rob, M. A.; Cheeseman, J. R.; Montgomery, J. A., Jr.; Vreven, T.; Kudin, K. N.; Burant, J. C.; Millam, J. M.; Iyengar, S. S.; Tomasi, J.; Barone, V.; Mennucci, B.; Cossi, M.; Scalmani, G.; Rega, N.; Petersson, G. A.; Nakatsuji, H.; Hada, M.; Ehara, M.; Toyota, K.; Fukuda, R.; Hasegawa, J.; Ishida, M.; Nakajima, T.; Honda, Y.; Kitao, O.; Nakai, H.; Klene, M.; Li, X.; Knox, J. E.; Hratchian, H. P; Cross, J. B.; Bakken, V.; Adamo, C.; Jaramillo, J.; Gomperts, R.; Stratmann, R. E.; Yazyev, O.; Austin, A. J.; Cammi, R.; Pomelli, C.; Ochterski, J. W.; Ayala, P. Y.; Morokuma, K.; Voth, G. A.; Salvador, P.; Dannenberg, J. J.; Zakrzewski, V. G.; Dapprich, S.; Daniels, A. D.; Strain, M. C.; Farkas, O.; Malick, D. K.; Rabuck, A. D.; Raghavachari, K.; Foresman, J. B.; Ortiz, J. V.; Cui, Q.; Baboul, A. G.; Clifford, S.; Cioslowski, J.; Stefanov, B. B.; Liu, G.; Liashenko, A.; Piskorz, P.; Komaromi, I.; Martin, R. L.; Fox, D. J.; Keith, T.; Al-Laham, M. A.; Peng, C. Y.; Nanayakkara, A.; Challacombe, M.; Gill, P. M. W.; Johnson, B.; Chen, W.; Wong, M. W.; Gonzalez, C.; Pople, J. A. *Gaussian 03*.

(19) The titration experiments demonstrated that **1**⁴⁺ and NO$_3$⁻ form the host–guest complex after addition of the anion to the DMSO-d_6 solution of **1**(OTf)$_4$.

(20) Aoyagi, M.; Biradha, K.; Fujita, M. *J. Am. Chem. Soc.* **1999**, *121*, 7457–7458.

(21) Examples: (a) Campos-Frnández, C. S.; Schottel, B. L.; Chifotides, H. T.; Bera, J. K.; Bacsa, J.; Koomen, J. M.; Russell, D. H.; Dunbar, K. R. *J. Am. Chem. Soc.* **2005**, *127*, 12909–12923.

(b) Hasenknopf, B.; Lehn, J.-M.; Boumediene, N.; Leize, E.; Dorsselaer, A. V. *Angew. Chem., Int. Ed.* **1998**, *37*, 3265–3268. (c) Hasenknopf, B.; Lehn, J.-M.; Boumediene, N.; Dupont-Gercais, A.; Dorsselaer, A. V.; Kneisel, B.; Fenske, D. *J. Am. Chem. Soc.* **1997**, *119*, 10956–10962.

(22) (a) Furlan, R. L. E.; Otto, S.; Sanders, J. K. M. *Proc. Natl. Acad. Sci. U. S. A.* **2002**, *99*, 4801–4804. (b) Davis, A. V.; Yeh, R. M.; Raymond, K. N. *Proc Natl. Acad. Sci. U. S. A.* **2002**, *99*, 4793–4796. (c) Leiniger, S.; Olenyuk, B.; Stang, P. J. *Chem. Rev.* **2000**, *100*, 853–908.

(23) ¹H NMR spectrum of the suspension exhibited none of the signals of (*n*-Bu)$_4$N⁺ (Figure 12b). This indicates that the concentration of (*n*-Bu)$_4$N⁺ in the reaction solution remained unchanged during the reaction.

(24) Thermal reaction of **1**(OTf)$_4$ (1.0 mM) with 4 equiv of OTs⁻ (4.0 mM) and NO$_3$⁻ (0.5 mM) as (*n*-Bu)$_4$N⁺ salts afforded **2**⊃(OTs|NO$_3$|OTs)⁵⁺ and **2**⊃(NO$_3$|NO$_3$|NO$_3$)⁵⁺. See Figure S12 in the Supporting Information. **1**(OTf)$_4$ was used as a starting material, as [**1**⊃(OTs)$_2$](OTs)$_2$ is barely soluble in DMSO-d_6.